Conference Paper, Author's Postprint

Ewers, Jeanne

Incipient motion of sand under combined flow and full-scale waves

Erstveröffentlichung in Uijttewaal, Wim S. J. et al. (Hrsg.) (2020): River Flow 2020. Proceedings of the 10th Conference on Fluvial Hydraulics (Delft, Netherlands, 7-10 July 2020), London, Great Britain, S. 984-992.

Incipient motion of sand under combined flow and full-scale waves

Jeanne Ewers[a]

[a] Federal Waterways Engineering and Research Institute (BAW)

Abstract: This experimental study was conducted to investigate the effects of pressure variations on sediment entrainment. A quasi-saturated fine sand sample was examined. In a closed-conduit, it was subjected to stream flow causing weak sediment movement. Full-scale waves were simulated by applying absolute pressure fluctuations at the sediment surface. The results prove that pressure variations cause vertical seepage in the bed. An absolute pressure reduction causes upward seepage. Image analysis of the bed surface reveals an increase of sediment mobility during pressure reduction. Data evaluation shows that this increase is mainly triggered by the upward seepage force acting on the particles.

1 Introduction

Waterway bank and bottom protections have multiple functions such as ensuring slope stability and erosion resistance. At the same time, they are habitat for flora and fauna and thus have an ecological function. Towards ecologically and technically improved bank and bottom protections a deepened understanding of the occurring physical phenomena caused by hydraulic loads at the river bed is fundamental. Hydraulic loads include stream flow, natural or ship-induced waves, and seepage processes in the soil. While conventional bank protections consist of revetments with rip-rap (Bundesanstalt für Wasserbau 2010), technical biological bank protections preferably work without armourstones. Accordingly, the stabilizing load is replaced by plants and roots. As the establishment of plants for technical-biological bank protections needs at least one growing season, the banks are only little stabilized in an initial time period. Thus, a deeper insight into the interactions between stream flow and ship-induced wave loading on the unstabilized banks and bottoms is necessary for enhanced bank protection measures.

Considering wave loading, the soil reactions in sandy river beds are analytically well understood (e.g. Biot 1941, Hsu & Jeng 1994) and have been analyzed experimentally, numerically and analytically in Ewers et al. (2017). Assuming that natural sandy river beds contain a small amount of gas, i.e. are quasi-saturated (Tarantino 2013), excess pore water pressures and seepage occur due to wave loading. Practically, inland vessels induce a rapid drawdown on the banks and bottoms of waterways leading to vertical upward seepage. As a consequence, the submerged weight of the single sand particles is reduced which means that the resistance of the particles against entrainment is reduced. Therefore, incipient motion analysis must consider wave-induced seepage.

Regarding the coupled analysis of stream flow and seepage occurrence, studies show that the presence of seepage has an effect on the boundary shear stress (Baldock & Holmes 1998, Francalanci et al. 2008). In the presence of vertical upward seepage the shear stress at the sediment surface is reduced (Lu et al. 2008). Hence, the main action on a single particle triggering sediment entrainment is reduced. As stated above the main resistance against entrainment is reduced at the same time. Cao et al. (2016) quote that the effect on sediment entrainment depends on the amplitude of the seepage force. This explains why a part of existing studies show an increase of the transport rate due to upward seepage while others document the opposite.

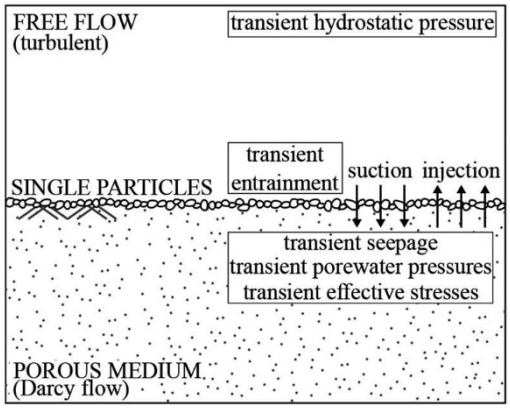

Figure 1: Boundary value problem.

Figure 1 Shows the three main components of the problem, turbultent free flow, porous medium with Darcy flow and the single soil particles at the interface. Due to transient hydrostatic pressures in the free flow area, the porous medium reacts with transient porewater pressures, effective stresses and seepage and transient particle entrainment.

The aim of this experimental study lies on the qualitative investigation of the observed interactions between time-dependent pressure-induced soil processes and free flow on the sediment motion process. The outline of the contribution consists of the theoretical framework, the description of the experiments carried out with the riverbed simulator and finally the presentation and interpretation of the results.

2 Theoretical Framework

2.1 Wave-induced soil mechanical processes in quasi-saturated sands

Waves are taken into account as water pressure variations at the bed surface. The sandy soil is considered as a two phase porous medium consisting of a soil skeleton and a pore fluid. It is assumed that sandy beds of waterways have a degree of saturation between 85 to 99% (Bundesanstalt für Wasserbau 2010). These saturation conditions are called quasi-saturated (Tarantino 2013) since the relatively small amount of gas bubbles in the pores can be incorporated to the fluid phase by an increased compressibility of the water-gas-mixture (Pietruszczak & Pande 1996). After Fredlund (1976) the compressibility of the water-gas-mixture is mainly a function of the degree of saturation

S and the absolute pressure *p*. It is significantly increased compared to that of water and is within the range of the soil stiffness.

The constitutive behavior of quasi-saturated sand depends on the deformation behavior of the soil skeleton and on the compressibility of the water-gas-mixture. A rapid water drawdown results in a lagged water pressure reaction in the bed causing excess pore water pressures and vertical upward hydraulic gradients and seepage forces in a near-surface area. If the hydraulic gradient exceeds a critical value the soil skeleton looses its shear strength and liquefaction occurs. The soil reactions depend predominantly on the compressibility of the pore fluid mixture and the permeability of the soil (Ewers & Karl 2017). If linear-elastic soil behavior is assumed the processes can be described by Biot's consolidation theory (Biot 1941), which implies small strains and the validity of Darcy's law. Darcy's law states a linear relation between seepage velocity q and hydraulic gradient i with $q = k \cdot i$ and depends on the permeability k. The hydraulic gradient is a function of excess pore water pressure Δp

$$i(z) = \frac{\Delta p(z)}{z \cdot \rho_w \cdot g} \tag{1}$$

with z the corresponding depth, ρ_w = 1 tm^{-3} the density of water and g =9.81 ms^{-2} the gravitational acceleration.

2.2 Seepage effects on sediment entrainment

In general, sediment entrainment is mainly driven by the bed shear stress induced by the main flow and depends on the submerged weight and size of the sand particles. The threshold condition of incipient motion without seepage can be estimated by the determination of the critical Shields parameter as a function of material and flow properties (Annandale 1995). Therefore, van Rijn (1984) defines a particle parameter

$$d_* = d_{\mathrm{char}} \left(\frac{\rho_s/\rho_w - 1}{\nu^2} \right)^{1/3} \tag{2}$$

depending on a characteristic particle diameter d_{char}, the bulk density of the bed particles ρ_s, and the kinematic viscosity ν. The critical Shields parameter is defined as

$$\Theta_{\mathrm{cr}} = \frac{u_{*,\mathrm{cr}}^2}{(\rho_s/\rho_w - 1) g d_{\mathrm{char}}} \tag{3}$$

with $u_{*,cr}$ the critical bed shear velocity according to Shields (1936). It is a function of bed shear stress.

Seepage flow has various effects on sediment entrainment. First, seepage modifies the bed shear stress. Second, seepage induces a change in submerged unit weight of the soil particles. Third, seepage affects the effective stresses in near-surface area of the bed. Those effects cause a change in the threshold condition of sediment entrainment, meaning that the critical Shields number changes, see Eq. (3). In the presence of vertical upward seepage or fluid injection (cf. Figure 1) to the main flow

the bed shear stress decreases (Liu & Chiew 2014). The mean main flow velocity increases due to the influx of mass and thus increases the bed shear stress indirectly (Francalanci et al. 2008, Baldock & Nielsen 2010). The submerged unit weight of the soil particles decreases (Cheng & Chiew 1999). The effective stresses decrease and thus the shear strength of the soil is reduced (Ewers 2018). Finally, it has an impact on turbulence intensities. However, the influence of seepage on turbulence intensity is not clearly understood (Lu et al. 2008).

As a whole, the impact of seepage on sediment entrainment cannot be deduced easily. In the case of injection the bed shear stress will be reduced, while at the same time it might be increasing due to the mass influx. The resistance of the soil particles is reduced. Looking at Eq. ((2)) d decreases. Considering Eq. (3) the change of Θ_{cr} is not easily established since it depends on the particle property and the critical shear velocity which is a function of critical shear stress. Existing studies show contradictory results of the seepage effects on sediment transport rate, bed shear stress and trubulence intensity (Lu et al. 2008).

Cao et al. (2016) introduce a closed-conduit flow study with fine to middle sand. A horizontal main flow close to the critical shear velocity with observed slow movement of single particles at the bed surface is used in combination with vertical upward seepage. They deduce a critical seepage velocity from a permeability test. It is defined as the critical seepage velocity q_{cr} where the relation between seepage velocity and hydraulic gradient becomes nonlinear invalidating Darcy's law. Cao et al.'s (2016) results show that the sediment transport rate increases significantly when the ratio of the applied vertical seepage velocity to the critical seepage velocity q/q_{cr} is greater than 10. For q/q_{cr} <10, the change in transport rate compared to the no-seepage case is negligible. Liu & Chiew's (2014) data is based on open channel experiments on coarse sand. They show the effect of injection on the transport rate with q/q_{cr} <1. In the experiments, the transport rate decreases slightly due to injection. Liu & Chiew (2014) and Cao et al. (2016) use a sand trap to measure the steady state transport rate within a defined time period. Cao & Chiew (2014) study the effects of suction (cf. Figure 1) on sediment transport in a closed-conduit on a coarse sand. They show that for small suction velocities the transport rate is not affected. For increasing suction velocities the transport rate increases rapidly.

3 River Bed Simulator Experiments

3.1 Testing facility

The tests were carried out with the river bed simulator of the BAW, shown in Figure 2. It is a newly developed recirculating closed-conduit flume with an integrated soil sample container. The flow cross section has a width of 0.4 m and a height of 0.2 m (cf. Figure 3). The soil sample has a depth of 1.2 m and an erosion surface length of 1.5 m. The facility is equipped with two pumps with a discharge up to 250 ls^{-1} generating a mean flow velocity of up to 3 ms^{-1} in the rectangular test section. In order to obtain a fully developed flow profile at the beginning of the test section the water is run through a flow damper, which consists of a baffle plate and two perforated plates, followed by a confuser and a rectangular flow inlet section of 8 m length.

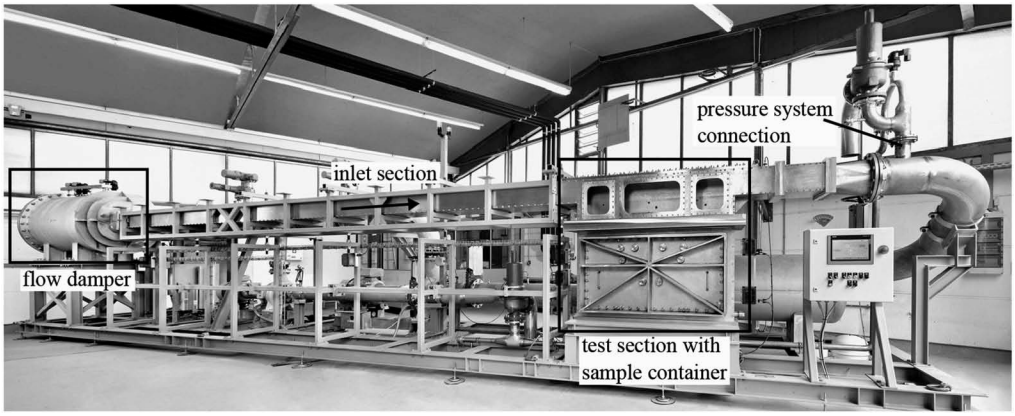

Figure 2: Front view of the Riverbed-Simulator.

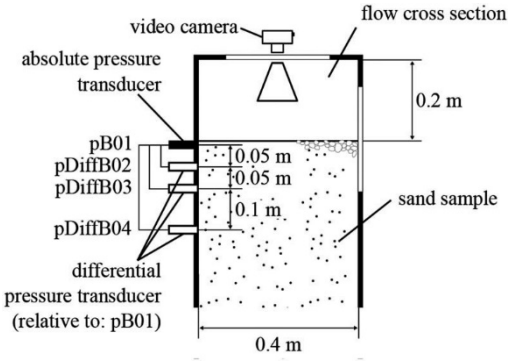

Figure 3: Cross sectional view of the sample container with pressure measurements and video recording.

The river bed simulator is connected to a pressure system described in Kayser et al. (2016). It applies absolute pressures up to 3 bar to the whole conduit, corresponding to 20 m water depth. It is possible to apply sinusoidal pressure fluctuations e.g. simulating Airy waves or linear pressure changes with amplitudes and periods at natural scale.

The facility is equipped with two magnetic flow meters behind the pumps and one at the conduit connecting the facility to the pressure system. As shown in Figure 3, a series of absolute and differential pressure transducers are installed in different depths of the test sample. The differential pressure transducers have a precision of 0.6 mbar (6 mm). The erosion process is monitored by a camera through a top viewing window (cf. Figure 3), recording the erosion surface and capturing the particle entrainment process with an aquisition rate of 50 Hz.

3.2 Soil material and sample preparation

In the presented study, a fine to middle quartz sand with a median particle diameter d_{50} of 0.18 mm and a high uniformity of $C_U = d_{60}/ d_{10} \approx 1.7$ has been used. The particle density is $\rho_s = 2.6$ tm^{-3}.

For the sample preparation, the dry sand is pluviated into standing water in the soil sample container. The relative density of the preparated soil sample has not been monitored. Earlier tests (Ewers & Karl 2017) suggest a medium dense to loose packing of the sample. In order to obtain quasi-saturated

conditions, the sand sample has been drained and slowly resaturated from the bottom two times. The mean degree of saturation can be determined based on the pressure and discharge measurements following the approach described in Ewers (2016). The resulting mean degree of saturation of the sample is $S \approx 90\%$ for an absolute pressure level of p = 2.26 bar. The permeability test performed by applying a vertical downward seepage through the sample container and measuring the discharge and pore water pressures gives a mean permeability of $k \approx 3.2 \cdot 10^{-4}$ ms^{-1}.

3.3 Image analysis

The video recording of the bed surface (c.f. Figure 3) shows the time dependent bed load movement of the single sand particles in an area of about 3 x 5 cm^2. It is evaluated by calculating the mean squared error

$$MSE = \frac{1}{n}\sum_{i=1}^{n}(Y_i - \hat{Y}_i)^2 \tag{4}$$

where (Y_i - $\hat{Y}_i$) is the difference of RGB-values in each pixel i between two subsequent frames. n corresponds to the pixel number of 1080 x 1920 px. It is an integral description of the similarity between two images and it is independent of the sign. On the basis of the available data, the result of the *MSE* gives a qualitative averaged measure of the change in transport rate in the observation area. A higher *MSE*-value indicates an increased transport rate. The evaluation was performed with a frequency of about 2 Hz equaling a given time increment of 0.5 seconds between two subsequent frames. In order to obtain a relative measure with reference to the undisturbed condition the *MSE* is related to the mean *MSE* of a certain time interval at the beginning of the measurement with constant pressure and flow velocity

$$MSE_{\mathrm{rel}} = \frac{MSE}{\overline{MSE}_{\mathrm{ref}}} \tag{5}$$

if $MSE_{\mathrm{rel}} \approx 1$ the sediment mobility is unchanged. For $MSE_{\mathrm{rel}} > 1$ it is increased.

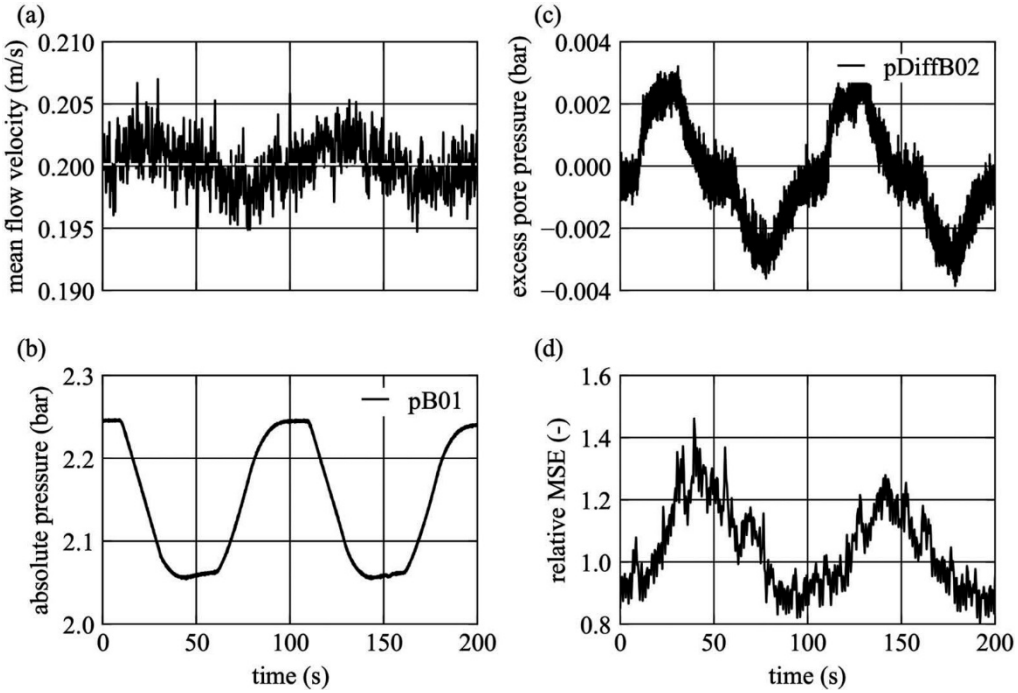

Figure 4. (a) Mean flow velocity in the flow cross section during the test (white dashed line: average). (b) Time-dependent pressure boundary condition at the erosion surface. (c) Excess pore water pressure at a depth of 0.05 m. (d) Result of the video analysis of the sediment mobility in terms of relative MSE (cf. Eqs. (4) and (5)).

3.4 Testing procedure

The presented experiment was carried out with a mean flow velocity in the flow cross section of about 0.2 ms^{-1} based on flowrate measurements, see Figure 4a. During the test, the pressure boundary condition at the erosion surface was varied. Figure 4b diplays the time-dependent pressure boundary condition at the sample surface (pB01 in Figure 3). The absolute pressure is decreased linearly by about 0.2 bar = 2 m water column within a time interval of about 20 s. Then, the pressure was held constant at this level for about 40 s and finally increased again to the initial level. The form of the linear lowering reproduces a simplified ship-induced drawdown at a waterway bank (Bundesanstalt für Wasserbau 2010). The amplitude and velocity of the pressure drop has been chosen in accordance to previous tests (Ewers & Karl 2017).

Visually, the initial sediment mobility with a constant mean flow velocity of 0.2 ms^{-1} and constant absolute pressure of 2.25 bar is in the range of incipient sediment motion. The classification relates to the description of weak particle movement following Kramer as described in Buffington (1999).

4 Results and Discussion

Figures 4a, b show the mean flow velocity and absolute pressure boundary condition. Figure 4c displays the excess pore water pressure at 0.05 m depth. During pressure drawdown the excess pore water pressure increases, followed by a consolidation phase during the constant pressure interval.

Then the process is reversed. The maximum excess pore pressure is about 0.003 bar = 0.03 m at the end of the drawdown of ≈ 2 m.

Figure 5 displays the dependency between seepage velocity and hydraulic gradient as defined in Eq. (1). The linear regression has a slope of $2.4 \cdot 10^{-4}$ ms^{-1} which corresponds to the near-surface permeability of the soil sample (cf. Darcy's law). It is similar to the result of the permeability test, see section 3.2. The linearity gives evidence that the sample is not liquefied due to the present pressure boundary condition (Ewers 2018).

Figure 4d shows the results of the image analysis in terms of relative MSE which increases during and after pressure drawdown. A change in the *MSE*-value is not observed during pressure increase. Figure 6 displays scatter plots of relative *MSE* as a function of the pressure boundary condition, the excess pore water pressure and the mean velocity. It suggests that the relative *MSE* is a function of the pressure boundary condition pB01 with increasing mobility during drawdown (Figure 6a). Figure 6b indicates that higher excess pore water pressures correlate with higher relative *MSE*-values. Figure 4c, d show that the excess pore water pressure increases rapidly during drawdown and reaches its peak directly at the end of the drawdown while the sediment mobility increase is slower and reaches its peak value slightly later. A dependency between mean main velocity and relative *MSE* cannot be shown (Figure 6c). The mean main flow is increased by the influx of water to the flow cross section which is an additional driver of sediment mobility (cf. Figure 4a). During pressure increase the main flow velocity is slightly decreased but no reaction in relative *MSE* is observed. Taken together, the main flow change is negligible.

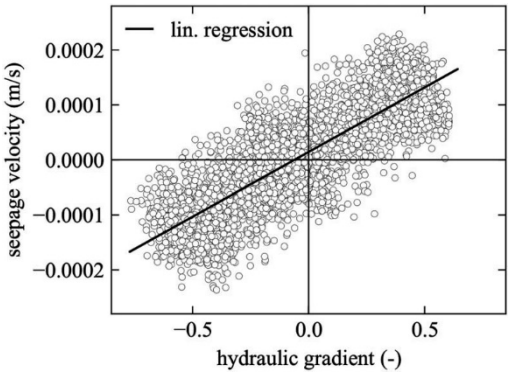

Figure 5. Seepage velocity at bed surface over hydraulic gradient at 0.025 m depth. The graph shows the linear regression and indicates the validity of Darcy's law with a permeability of $2.4 \cdot 10^{-4}$ ms^{-1}.

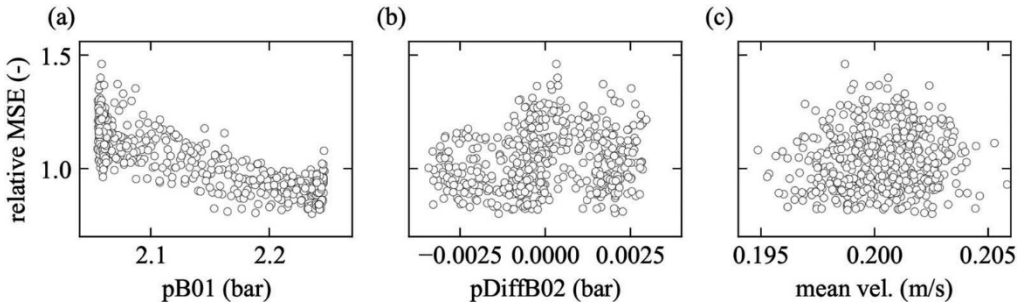

Figure 6. Scatter plots of the rel. MSE with respect to the pressure boundary condition pB01, the excess pore water pressure pDiff02 and the mean main velocity.

Cao et al. (2016) state that the effect of injection on the bed-load transport rate results in increased transport rates if the injection intensity q/q_{cr} is greater 10. As shown in Figure 5 the linearity between hydraulic gradient and seepage velocity is valid and therefore q_{max}/q_{cr} <1 for the test case. Hence, the observed phenomenon of an increase in mobility is not in accordance to the observations of Cao et al. (2016). In order to explain this discrepancies, further analysis and a quantitative measure for the transport rate is necessary. Furthermore, a difference may arise from the fact that the presented experiment investigates time-dependent processes while Cao et al. analyse static phenomena.

5 Conclusion

The newly developed river bed simulator is a closed-conduit flow facility with applicable pressure boundary conditions at natural scale. This allows for the analysis of near-natural wave-induced soil processes and their effects on sediment entrainment.

The presented experimental study shows the basic response of a quasi-saturated sand sample to main flow and linear pressure changes. The data evaluation shows that the sediment mobility increases during pressure draw down. This can be traced back to the fact that vertical upward seepage acts as an additional destabilizing force on the single particle at the bed surface resulting in a reduced resistance of the single particle to entrainment. Here, this effect is the triggering effect of the increased sediment mobility. At the same time, it is known that vertical upward seepage reduces the bed shear stress. Since sediment mobility is enhanced, this is not the decisive effect. Also the main flow change due to mass influx is not the triggering effect for increasing sediment mobility. During pressure increase and vertical downward seepage, a change in sediment mobility is not observed. Further experiments with variation of pressure boundary conditions and seepage forces are planned to quantitatively investigate the described phenomena.

Acknowledgment

I thank Fabian Karl who provided insight and expertise in the experimental approach, measurement techniques and valuable discussions that assisted the research.

References

Annandale, G.W. 1995. Erodibility. Journal of Hydraulic Research 33(4):471–494.

Baldock, T. & Holmes P. 1998. Seepage effects on sediment transport by waves and currents. Coastal Engineering 3601–3614.

Baldock, T. & Nielsen, P. 2010. Discussion of "Effect of Seepage-Induced Nonhydrostatic Pressure Distribution on Bed-Load Transport and Bed Morphodynamics" by Simona Francalanci, Gary Parker, and Luca Solari. Journal of Hydraulic Engineering 136(1): 77–79.

Biot, M.A. 1941. General Theory of Three-Dimensional Consolidation. Journal of Applied Physics 12(2): 155–164.

Buffington, J.M. 1999. The Legend of A. F. Shields. Journal of Hydraulic Engineering 125(4): 376–387. Bundesanstalt für Wasserbau (BAW) (ed.) 2010. Principles for the Design of Bank and Bottom Protection for Inland Waterways (GBB). BAW Code of Practice. Issue 2010. Karlsruhe: Bundesanstalt für Wasserbau.

Cao, D.P. & Chiew, Y.M. 2014. Suction Effects on Sediment Transport in Closed-Conduit Flows. Journal of Hydraulic Engineering 140(5): 4014008.

Cao, D.P., Chiew, Y.M., & Yang, S.Q. 2016. Injection Effects on Sediment Transport in Closed-Conduit Flows. Acta Geophysica 64(1): 125â€"148.

Cheng, N.-S. & Chiew, Y.-M. 1999. Incipient sediment motion with upward seepage. Journal of Hydraulic Research 37(5): 665–681.

Ewers, J. 2016. Porenströmung als Auslöser für Erosion? Does Seepage in Porous Beds Trigger Incipient Motion? In Bundesanstalt für Wasserbau (ed.), BAWMitteilungen. Johann-Ohde-Kolloquium, 99: 45–56, Karlsruhe.

Ewers, J. 2018. Laboratory tests on the effects of wave action on cohesionless soil and their influence on incipient sediment motion. In: Yeh Keh-Chia (ed.) Scour and Erosion IX. Proceedings of the 9th Inter- national Conference on Scour and Erosion (ICSE 2018), November 5-8, 2018, Taipei, Taiwan 9: 511–518. Taylor & Francis.

Ewers, J. & Karl, F. 2017. Determining Fluid Compressibility and Soil Permeability of Quasi Saturated Sand with the Alternating Flow Apparatus. In: Alessio Ferrari und Lyesse Laloui (eds). Advances in Laboratory Testing and Modelling of Soils and Shales (ATMSS). International Workshop Cham, Switzerland: Springer (Springer Series in Geomechanics and Geoengineering).

Ewers, J., Sorgatz, J., & Montenegro, H. 2017. Laborversuche und gekoppelte Berechnungen zur Untersuchung von Porenwasserüberdrücken infolge schneller Wasserstandsabsenkungen. In: Deutsche Gesellschaft für Geotechnik (ed.). Fachsektionstage Geotechnik. Interdisziplinäres Forum. 1(1): 400–405.

Francalanci, S., Solari, L., & Parker, G. 2008. Effect of Seepage-Induced Nonhydrostatic Pressure Distribution on Bed-Load Transport and Bed Morphodynamics. Journal of Hydraulic Engineering 134(4): 378–389.

Fredlund, D.G. 1976. Density and compressibility characteristics of air–water mixtures. Canadian Geotechnical Journal 13(4): 386–396.

Hsu, J.R.C. & Jeng, D.S. 1994. Wave-induced soil response in an unsaturated anisotropic seabed of finite thickness. International Journal for Numerical and Analytical Methods in Geomechanics 18(11):785–07.

Kayser, J., Karl, F., SchÃ¼renkamp, D., Schwab, N., & Oumeraci, H. 2016. A Test Apparatus for Alternating Flow in Geotechnical Engineering. Geotechnical Testing Journal 39(5): 865–878.

Liu, X. & Chiew, Y.M. 2014. Effect of upward seepage on bedload transport rate. Water Science and Engineering 7(2): 208–217.

Lu, Y., Chiew, Y.M., & Cheng, N.S. 2008. Review of seepage effects on turbulent open-channel flow and sediment entrainment. Journal of Hydraulic Research 46(4): 476–488.

Pietruszczak, S. & Pande, G.N. 1996. Constitutive Relations for Partially Saturated Soils Containing Gas Inclusions. Journal of Geotechnical Engineering 122(1): 50–59.

Shields, A. 1936: Anwendung der Ähnlichkeitsmechanik und der Turbulenzforschung auf die Geschiebebewegung. Mitteilungen der Preußischen Versuchsanstalt für Wasserbau und Schiffbau, Dissertation 26. Berlin.

Tarantino, A. 2013. Basic Concepts in the Mechanics and Hydraulics of Unsaturated Geomaterials. In Lyesse Laloui (ed.), Mechanics of Unsaturated Geomaterials London: Wiley.

van Rijn, L.C. 1984. Sediment Transport, Part I. Bed Load Transport. Journal of Hydraulic Engineering 110(10): 1431–1456.

Author:

Jeanne Ewers
Federal Waterways Engineering and Research Institute (BAW)
Kußmaulstraße 17, 76187 Karlsruhe
E-Mail: jeanne.ewers@baw.de.